



## The current status of the GRAPES-3 extensive air shower experiment

S.K. Gupta<sup>a</sup>, H.M. Antia<sup>a</sup>, S.R. Dugad<sup>a</sup>, U.D. Goswami<sup>a</sup>, Y. Hayashi<sup>b</sup>, A. Iyer<sup>a</sup>, N. Ito<sup>b</sup>, P. Jagadeesan<sup>a</sup>, A. Jain<sup>a</sup>, S. Karthikeyan<sup>a\*</sup>, S. Kawakami<sup>b</sup>, M. Minamino<sup>b</sup>, P.K. Mohanty<sup>a</sup>, S.D. Morris<sup>a</sup>, P.K. Nayak<sup>a</sup>, T. Nonaka<sup>b</sup>, A. Oshima<sup>a</sup>, B.S. Rao<sup>a</sup>, K.C. Ravindran<sup>a</sup>, H. Tanaka<sup>a</sup>, S.C. Tonwar<sup>a</sup>  
(The GRAPES-3 Collaboration)

<sup>a</sup>Tata Institute of Fundamental Research, Mumbai 400005, India

<sup>b</sup>Graduate School of Science, Osaka City University, Osaka 558-8585, Japan

The GRAPES-3 is a dense extensive air shower array operating with  $\sim 400$  scintillator detectors and it also contains a 560 m<sup>2</sup> tracking muon detector ( $E_\mu > 1$  GeV), at Ooty in India. 25% of scintillator detectors are instrumented with two fast photomultiplier tubes (PMTs) for extending the dynamic range to  $\sim 5 \times 10^3$  particles m<sup>-2</sup>. The scintillators, signal processing electronics and data recording systems were fabricated in-house to cut costs and optimize performance. The muon multiplicity distribution of the EAS is used to probe the composition of primary cosmic rays below the ‘knee’, with an overlap with direct measurements. Search for multi-TeV  $\gamma$ -rays from point sources is done with the aid of the muon detector. A good angular resolution of 0.7° at 30 TeV, is measured from the shadow of the Moon on the isotropic flux of cosmic rays. A sensitive limit on the diffuse flux of 100 TeV  $\gamma$ -rays is placed by using muon detector to filter the charged cosmic ray background. A tracking muon detector allows sensitive measurements on coronal mass ejections and solar flares through Forbush decrease events. We have major expansion plans to enhance the sensitivity of the GRAPES-3 experiment in the areas listed above.

### 1. Introduction

The GRAPES-3 (**G**amma **R**ay **A**stronomy at **P**eV **E**nergie**S**- phase **3**) is a high density extensive air shower (EAS) array designed for a precision study of the cosmic ray (CR) energy spectrum and its nuclear composition using the muon multiplicity distribution (MMD) in the energy range from  $3 \times 10^{13}$  eV to  $3 \times 10^{16}$  eV [1]. The experiment was started with 256 plastic scintillator detectors (each 1 m<sup>2</sup> in area) deployed on a dense hexagonal pattern with an inter-detector separation of 8 m, at Ooty (2200 m altitude, 11.4°N, 76.7°E) in south India in 2001 as shown in Fig. 1 [2]. The array also contains a large area (560 m<sup>2</sup>) tracking muon telescope [3] to measure the muon component and obtain the MMD of the EAS. The muon telescope has also provided new information on solar flares, coronal mass ejections and Forbush decrease (Fd) events [4,5].

The occurrence of the ‘knee’ in the CR energy spectrum around  $3 \times 10^{15}$  eV is believed to be in-

timately linked to the issue of CR origin. But even after several decades of study, a clear understanding of the origin of the ‘knee’ is yet to emerge. Data obtained with higher sensitivity and less uncertainty in the estimate of primary energy and composition are expected to provide a better understanding of this important feature of the high energy astrophysics.

Solar flares accelerate charged particles through a variety of mechanisms, which may be constrained through observations at high energies ( $> 10$  GeV). We searched for direct emission of protons of energy  $\gtrsim 20$  GeV in association with an X17 class solar flare that occurred on 28 October 2003, using a large area tracking muon telescope. A 99% C.L. upper limit on the flux of protons due to the solar flare was placed at  $1.4 \times 10^{-6}$  cm<sup>-2</sup>s<sup>-1</sup>sr<sup>-1</sup>, nearly two orders of magnitude lower than flux values reported earlier for other flares. New information on the structure and time evolution of the large Fd observed on 29 October 2003 from nine different solid angle bins ( $\sim 0.3$  sr) showed a remarkably similar behavior,

\*deceased

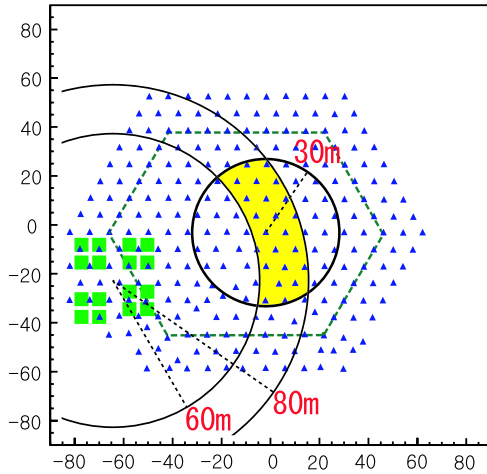


Figure 1. The GRAPES-3 array with 257 detectors ( $\blacktriangle$ ) and 16 muon detector modules ( $\blacksquare$ ).

with an evolution on a time scale of  $\sim 1$  h.

An efficient detector system should provide a large separation between the PMT noise and the signal from the charged particles in an EAS, and should also have a uniform spatial response over the entire area of the scintillator. The original GRAPES-3 trapezoidal shaped detectors, suffered from sizable non-uniformity and delivered a relatively small signal. Therefore, in the new detectors wave-length shifting (WLS) fibers are used to ensure a large signal, uniform response and a dynamic range of up to  $\sim 5 \times 10^3$  particles  $\text{m}^{-2}$ . The response of the detector was compared with the results of detailed Monte Carlo simulations to obtain a comprehensive understanding of the entire system [6].

The signal processing involves amplification and shaping of the PMT signal into a digital pulse. The necessary amplifiers and discriminator circuits were also developed and fabricated in-house and an accuracy of 100 ps was achieved in timing shower particles. The arrival time of individual detector signals are measured using time to digital converters (TDCs) developed in-house using the TDC32 ASIC developed by CERN. A time resolution of 500 ps with excellent linear-

ity and a dynamic range of 1 ms was achieved which matched the design capability of TDC32. Subsequently we have developed new 32 channel TDCs using the HPTDC ASIC from CERN, which allows a time resolution of 100 ps. The signal processing electronics for the muon detector is relatively simple because of the slower signals from the proportional counters. The entire data recording electronics for both the muon detector and the air shower array was also developed. This emphasis on in-house development has the following advantages, namely, (i) a significant reduction in cost, (ii) optimization and customization of the system according to the experimental requirements, (iii) fast repair in cases of failure, which is very important due to the remote location of Ooty.

## 2. Experimental details

In order to achieve the lowest possible energy threshold, a simple 3-line coincidence of detectors has been used to generate the Level-0 trigger, which acts as the fast GATE and START for the analog to digital converters (ADCs) and TDCs, respectively. As expected, this trigger selects a large number of very small and local showers and also larger showers whose cores land very far from the area covered by the array. Therefore, it is also required that at least 10 out of the inner 127 detectors should have triggered their discriminators within  $1 \mu\text{s}$  of the Level-0 trigger. This Level-1 trigger with an observed EAS rate of 13 Hz is used to record the charge (ADC) and the arrival time (TDC) of the pulses from each detector [2]. With the expansion of the array the trigger rate has increased to 30 Hz. The pulse charge is later converted into the equivalent number of minimum-ionizing particles (MIPS) using the most probable charge for a single MIP measured. The high sensitivity of scintillator detectors allows the atmospheric radon decay products to be routinely detected during every episode of rain in Ooty.

Fig. 1 also shows 16 squares in lower left side. Each square represents a 4-layer tracking muon telescope module with an energy threshold of 1 GeV for vertical muons. Each layer consists of 58 proportional counters, each 6 m long with

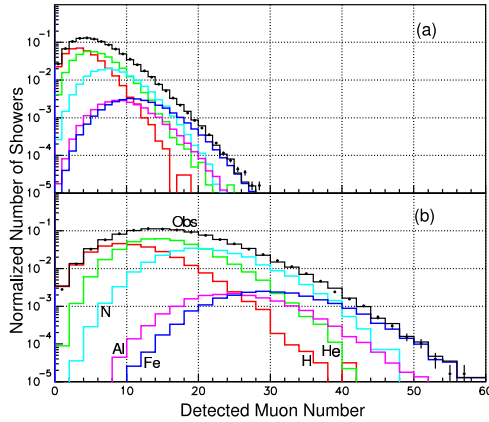


Figure 2. Observed muon multiplicity as histogram in black for, (a)  $10^{4.4} \leq N_e \leq 10^{4.6}$ , (b)  $10^{5.0} \leq N_e \leq 10^{5.2}$  for 5 component based SIBYLL generator.

$10 \times 10 \text{ cm}^2$  cross-sectional area. The  $560 \text{ m}^2$  GRAPES-3 muon telescope consists of 4 super-modules, each in turn having 4 modules. The muon energy threshold of 1 GeV is achieved by placing concrete of thickness  $\sim 550 \text{ g.cm}^{-2}$  above the muon telescope.

To improve the angular resolution of GRAPES-3, it was necessary to decrease the inter-detector separation in the array. This approach provides an excellent compromise between a small area carpet array and a very large area sparsely instrumented array. However, economic constraints limit the density of detectors employed in an EAS array. In the Tibet  $AS\gamma$  [7], CASA [8], EAS-TOP [9], KASCADE [10] and GAMMA [11] arrays, the area covered by the detectors is  $\lesssim 1\%$  of the physical area over which the array is spread. The density of detectors is a key factor that determines the measurement accuracy of parameters, such as the shower size ‘ $N_e$ ’ and arrival direction. The GRAPES-3 array is designed to have a dense configuration with a detector coverage of  $\sim 2\%$  of the array’s total area [2].

The angular resolution of GRAPES-3 has been measured by analyzing EAS data collected in 4 years and by using 3 different methods, namely,

even-odd, left-right and the shadow of the Moon. In the first method the array is divided into two sub-arrays of even and odd numbered detectors; in the second method the concept of left and right half-arrays with a cone-shaped shower front is used to estimate the energy dependent angular resolution of array. We measured a resolution of  $0.5^\circ$  for the left-right case which is marginally larger than  $0.4^\circ$  for the even-odd method for EAS of  $\geq 80 \text{ TeV}$ . Reduction in isotropic flux of CRs due to the shadow of Moon yields a resolution of  $0.5^\circ$  at  $\geq 80 \text{ TeV}$  [12].

### 3. GRAPES-3 Results

In the following we summarize the results obtained from the GRAPES-3 experiment on the primary composition, diffuse  $\gamma$ -ray emission, and on solar flares.

#### 3.1. Primary Composition

We have analyzed  $6 \times 10^8$  EAS collected over a live-time of  $5 \times 10^7 \text{ s}$ , for shower size  $N_e$ , core location  $(X_0, Y_0)$ , age ‘s’ by fitting the NKG function [13] to the lateral distribution. The EAS core is restricted to 30 m from the centre of array and a condition  $\theta < 45^\circ$  is imposed. The MMD is obtained for different  $N_e$  groups in intervals of 0.2 in  $\log_{10}(N_e)$ . A further cut on the distance of the EAS core, to lie between 60 to 80 m, from the centre of muon detector is imposed, as shown by the shaded area in Fig. 1. Monte Carlo simulations of EAS are carried out using the CORSIKA code [14] for 5 nuclei, namely, H, He, N, Al, and Fe. These simulations show that an efficiency of  $\sim 90\%$  is reached at 50 TeV for H and at 100 TeV for the Fe primaries [2]. The hadronic interactions in the simulations are described by the SIBYLL [15] and QGSJET [16] generators.

The MMD is also simulated for each of the 5 components using SIBYLL and QGSJET generators for the same range of  $N_e$  as the data. The contribution of each nuclear group is extracted by using a minimization technique described in [17]. The observed MMD is shown in Fig. 2a, as black histogram for shower size range,  $10^{4.4} \leq N_e \leq 10^{4.6}$ . Also shown in Fig. 2a are the contributions of 5 components, namely, p, He, N,

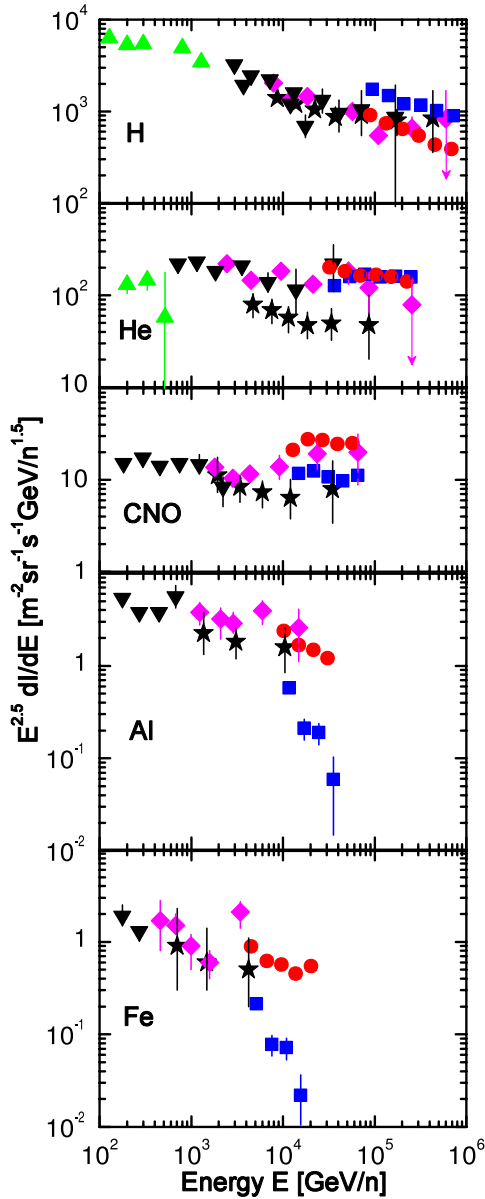


Figure 3. H, He, CNO, Al, Fe spectra from direct measurements  $\blacktriangle$  Ryan [18],  $\blacktriangledown$  SOKOL [19],  $\blacklozenge$  JACEE [21],  $\star$  RUNJOB [22], and GRAPES-3  $\bullet$  SIBYLL,  $\blacksquare$  QGSJET.

Al, Fe, simulated using SIBYLL. Fig. 2b shows

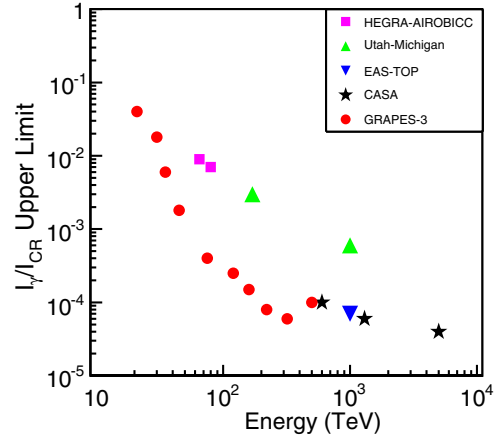


Figure 4. Diffuse  $\gamma$ -ray flux upper limits

the corresponding data and simulation results for size range,  $10^{5.0} \leq N_e \leq 10^{5.2}$ . The simulations are used to convert the size into the CR primary energy. The 5 component composition extracted from MMD distributions is shown in Fig. 3 for the QGSJET (filled squares) and SIBYLL (filled circles). These energy spectra are compared with the results from the direct observations also shown in Fig. 3. H and He data are taken from [18,19,21,22], and CNO, Al, Fe data from [19,20,22]. The GRAPES-3 data agree better with the direct measurements when SIBYLL generator is used, indicating that SIBYLL provides a good description of the hadronic interactions below 1 PeV.

### 3.2. Diffuse $\gamma$ -ray limits

The diffuse flux of  $\sim 100$  TeV  $\gamma$ -rays is produced from a variety of astrophysical sources, including the interactions of extremely high energy CRs with the 2.7°K cosmic microwave background (CMB) radiation. These interactions transfer the energy of CRs into  $\gamma$ -rays of progressively lower energy that in turn produce  $e^+ e^-$  pairs in the CMB field until the center of mass energy drops below the pair production threshold which occurs at ultra-high energies (UHE,  $E_\gamma \lesssim 10^{14} \text{eV} = 100$  TeV) and then the universe becomes relatively transparent to the propagation of UHE  $\gamma$ -rays.

Thus a pileup of  $\gamma$ -rays at  $\sim 100$  TeV is expected. More exotic scenarios such as the collapse of topological defects created in the early universe could also result in copious production of 100 TeV  $\gamma$ -rays.

Several groups in recent times have placed stringent upper limits on the diffuse  $\gamma$ -ray flux in the several tens of TeV to PeV ( $10^{15}$  eV) energy region which seem to question the validity of certain models of production of the highest energy particles. We have searched for diffuse  $\gamma$ -rays using the GRAPES-3 large area ( $560 \text{ m}^2$ ) muon telescope ( $E_\mu \geq 1 \text{ GeV}$ ). EAS with cores incident within the array and unassociated with penetrating tracks in the muon telescope, classified as  $\mu$ -poor, are considered as candidate  $\gamma$ -ray events. The  $\mu$ -poor cut was devised with the aid of simulations of CR and  $\gamma$  initiated EAS. In Fig. 4 the limits on the ratio  $I_\gamma/I_p$  of the intensities of  $\gamma$ -rays and CRs, respectively, are shown as a function of the primary energy. Also shown are the results reported by other groups [23–26].

### 3.3. Solar flare

We had searched for direct emission of protons of energy  $\gtrsim 20 \text{ GeV}$  in association with an X17 class solar flare on 28 October 2003. The tracking capability of the muon telescope allowed the field of view to be segmented into 9 bins, (labeled NE, E, SE, N, V, S, NW, W, SW; N north, E east, W west, S south and V vertical direction) each covering a solid angle of  $\sim 0.3 \text{ sr}$ . The large muon rate of  $3 \times 10^6 \text{ min}^{-1}$  permits a high precision study of various solar phenomena. Since detected  $>1 \text{ GeV}$  muons are secondaries of primary protons of  $\gtrsim 20 \text{ GeV}$  energy, we used these observations to place a 99% C.L. upper limit of  $1.4 \times 10^{-6} \text{ cm}^{-2} \text{ s}^{-1} \text{ sr}^{-1}$  on the wide-angle ( $\sim 2.5 \text{ sr}$ ) flux of solar protons. This limit is displayed in Fig. 5 along with results of other groups, including from neutron monitors (NMs) and GOES data. Using the muon telescope tracking feature a limit of  $4 \times 10^{-6} \text{ cm}^{-2} \text{ s}^{-1} \text{ sr}^{-1}$  is placed on the proton emission along a narrow beam ( $\sim 0.3 \text{ sr}$ ).

New information was obtained on the structure and time evolution of Fd observed on 29 October 2003 by GRAPES-3 [4]. The onset of Fd in 9 solid angle bins ( $\sim 0.3 \text{ sr}$ ) shows a remarkably similar

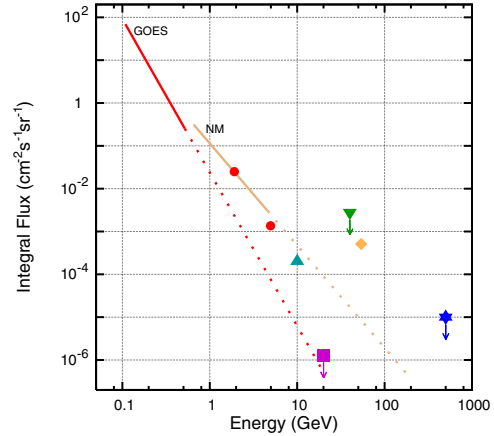


Figure 5. Integral protons flux data on 28 Oct 2003; (a) 100-600 MeV GOES-10/11 and sub-GeV balloon, (b) NM, (c)  $\gtrsim 20 \text{ GeV}$  GRAPES-3 limit, (d)  $\blacktriangle > 10 \text{ GeV}$  AGASA 4 Jun 1991, (e)  $\blacktriangledown > 40 \text{ GeV}$  L3 limit 14 Jul 2000, (f)  $\star > 500 \text{ GeV}$  Baksan limit on 29 Sep 1989, (g)  $\bullet$  NM 15 Apr 2001, (h)  $\blacklozenge$  NM 23 Feb 1956.

behavior, with an evolution on a time scale of  $\sim 1 \text{ h}$ . The observed muon rates in intervals of 6 min for the 9 bins are shown in Fig. 6. There is a systematic variation in time, when a specific feature in muon rate appears in a given solid angle bin. To highlight this aspect, the data in Fig. 6 are displayed after a grouping in 3 sets labeled “East”, “Center”, and “West”, respectively. The East set contains data from 3 eastern solid angle bins, namely, NE, E, and SE. Similarly the Center set contains data from bins N, V, S, and finally the West set contains NW, W, SW. For clarity, data shown in Fig. 6 for the Center and West sets have been shifted downwards by 4% and 8%, relative to East set. The 3 triangles in Fig. 6, indicate time of Fd minimum for each set. A power law dependence of magnitude of Fd on the cutoff rigidity was observed from the muon data over the range 14.3-24.0 GV, and we precisely measured the spectral slope to be  $\gamma = 0.53 \pm 0.04$ .

### 4. Future Plans

We propose to expand the GRAPES-3 array to detect CRs up to  $10^{18} \text{ eV}$  with the addition

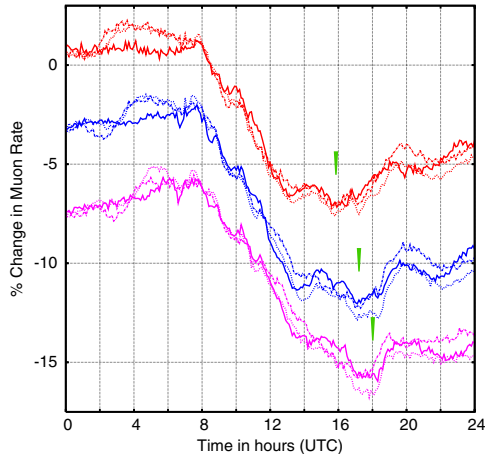


Figure 6. Variation in muon rate on 29 October 2003 from 9 solid angle bins grouped into 3 sets; east (NE, E, SE), center (N, V, S), and west (NW, W, SW). Successive sets shifted downwards by 4% for clarity. Each pointer represents time of Fd minimum for the 3 sets, respectively.

of new widely spaced detectors. We would also double the area of the muon detector to increase sensitivity for detecting  $\gamma$ -rays. The addition of an imaging Čerenkov telescope to measure the energy of primary CRs is also being contemplated. Setting up a neutron monitor to supplement information from the muon detector for solar studies is also being considered. Several new groups from within India have joined the collaboration and some from abroad are in the process of joining us.

### Acknowledgment

We thank D.B. Arjunan, G.P. Francis, I.M. Haroon, V. Jeyakumar, K. Manjunath, S. Murugapandian, B. Rajesh, K. Ramadass, C. Ravindran, V. Santosh Kumar and R. Suresh Kumar, V. Viswanathan for their help in the installation and operation of the experiment.

### REFERENCES

1. S.K. Gupta et al., Phys. Rev. D68 (2003) 052005.
2. S.K. Gupta et al., Nucl. Instr. Meth. A 540 (2005) 311.
3. Y. Hayashi et al., Nucl. Instr. Meth. A 545 (2005) 643.
4. T. Nonaka et al., Phys. Rev. D74 (2006) 052003.
5. P. Subramanian et al., To appear in Astron. Astrophys. (2009).
6. P.K. Mohanty et al., Astropart. Phys. 31 (2009) 24.
7. M. Amenomori et al., Nucl. Instr. Methods A 288 (1990) 619.
8. A. Borione et al., Nucl. Instr. Methods A 346 (1994) 329;
9. M. Aglietta et al., Astropart. Phys. 3 (1995) 1.
10. T. Antoni et al., Nucl. Instr. Methods A 513 (2003) 490.
11. Y.A. Gallant et al., Proc. 29th Int. Cosmic Ray Conf. Pune 4 (2005) 85.
12. A. Oshima et al., To be submitted to Astropart. Phys. (2009).
13. K. Greisen, Ann. Rev. Nucl. Sci. 10 (1960) 63.
14. D. Heck et al., Report, FZKA 6019, Forschungszentrum Karlsruhe (1998).
15. R.S. Fletcher et al., Phys. Rev. D 50 (1994) 5710.
16. N.N. Kalmykov et al., Nucl. Phys. B Proc. Suppl. 52 (1997) 17.
17. H. Tanaka et al., GRAPES-3 Preprint (2006).
18. M.J. Ryan et al., Phys. Rev. Lett. 28 (1972) 985.
19. I.P. Ivanenko et al., Proc. 23rd ICRC (Calgary) 2 (1993) 17.
20. K. Kobayakawa et al., Phys. Rev. D 66 (2002) 083004.
21. K. Asakimori et al., Astrophys. J. 628 (2005) L41.
22. V.A. Derbina et al., Astrophys. J. 502 (1998) 278.
23. J. Mathews et al., Astrophys. J. 375 (1991) 202.
24. A. Karle et al., Phys. Lett. B 347 (1995) 161.
25. M. Aglietta et al., Astroparticle Phys. 6 (1996) 71.
26. M.C. Chantell et al., Phys. Rev. Lett. 79 (1997) 1805.